High-Stable Lead-Free Solar Cells Achieved by Surface Reconstruction of Quasi-2D Tin-Based Perovskites

Feng Yang, Rui Zhu,* Zuhong Zhang, Zhenhuang Su,* Weiwei Zuo, Bingchen He, Mahmoud Hussein Aldamasy, Yu Jia, Guixiang Li,* Xingyu Gao, Zhe Li, Michael Saliba, Antonio Abate, and Meng Li*

Tin halide perovskites are an appealing alternative to lead perovskites. However, owing to the lower redox potential of Sn(II)/Sn(IV), particularly under the presence of oxygen and water, the accumulation of Sn(IV) at the surface layer will negatively impact the device's performance and stability. To this end, this work has introduced a novel multifunctional molecule, 1,4-phenyldimethylammonium dibromide diamine (phDMADBr), to form a protective layer on the surface of Sn-based perovskite films. Strong interactions between phDMADBr and the perovskite surface improve electron transfer, passivating uncoordinated Sn(II), and fortify against water and oxygen. In situ grazing incidence wide-angle X-ray scattering (GIWAXS) analysis confirms the enhanced thermal stability of the quasi-2D phase, and hence the overall enhanced stability of the perovskite. Long-term stability in devices is achieved, retaining over 90% of the original efficiency for more than 200 hours in a 10% RH moisture N_2 environment. These findings propose a new approach to enhance the operational stability of Sn-based perovskite devices, offering a strategy in advancing lead-free optoelectronic applications.

1. Introduction

Perovskite solar cells (PSCs) certified power conversion efficiency (PCE) of 26.1%, positioning them at the forefront of emerging solar cell technologies.[1–3] However, concerns regarding the toxicity of lead (Pb) and the environmental hazards associated with commercial production and large-scale applications have sparked interest in developing sustainable Pb-free PSCs.[4,5] Among the Pb-free candidates, tin (Sn) perovskites have emerged as a promising alternative due to their appropriate optical bandgap and high carrier mobility.[6,7] Also, Sn perovskites have shown steady improvements toward achieving high photovoltaic efficiencies.[8] In contrast to the Pb(II), which contains inert 6s electrons due to the relativistic effect making the Pb(II) cation chemically stable, the Sn(II)

F. Yang
Henan Key Laboratory of Photovoltaic Materials
School of Physics
Henan Normal University
Xinxiang 453007, China

F. Yang, R. Zhu, Z. Zhang, Y. Jia, M. Li
Key Lab for Special Functional Materials of Ministry of Education
National & Local Joint Engineering Research Center for High-efficiency
Display and Lighting Technology
School of Materials Science and Engineering
Collaborative Innovation
Center of Nano Functional Materials and Applications
Henan University
Kaifeng 475004, China
E-mail: zhurui@henu.edu.cn; mengli@henu.edu.cn

Z. Su, B. He, X. Gao
Shanghai Synchrotron Radiation Facility (SSRF)
Shanghai Advanced Research Institute
Chinese Academy of Sciences
239 Zhangheng Road, Shanghai 201204, P. R. China
E-mail: suzh@sari.ac.cn

W. Zuo, M. Saliba
Institute for Photovoltaics (*ipv*)
University of Stuttgart
Pfaffenwaldring 47, D-70569 Stuttgart, Germany

M. H. Aldamasy, G. Li, A. Abate
Helmholtz-Zentrum Berlin für Materialien und Energie GmbH
Hahn-Meitner-Platz 1, 14109 Berlin, Germany
E-mail: guixiang.li@epfl.ch

G. Li, A. Abate
Department of Chemistry
Bielefeld University
Universitätsstraße 25, 33615 Bielefeld, Germany

G. Li
Institute of Chemical Sciences and Engineering
École Polytechnique Fédéralede Lausanne (EPFL)
Lausanne 1015, Switzerland

cation's 5s electrons are more reactive, making the Sn(II) cation more susceptible to oxidation.[9] As a result, during the fabrication of the perovskite film, the Sn(II) cation at the B-site loses its 5s electrons easily, thus being oxidized to Sn(IV) upon exposure to any oxidation source such as oxygen, water molecules, or solvent with oxidation characteristics such as DMSO.[10,11] The uncontrolled redox activity triggers the Sn(II) oxidation, this occurs especially at the top surface of the perovskite's film, as the Fermi level of the perovskite is noticeably shallower than that of the electron contact (i.e., C_{60}).[12,13] As a result, tin perovskite devices show severe instability and high interfacial recombination rates, leading to hampered photovoltaic performance compared to lead perovskites.[14,15] It is evident that the inferior environmental stability of Sn perovskites under operation conditions, especially their sensitivity to oxygen, moisture, and temperature, has been a significant challenge for application into solar cells.[16,17]

Therefore, potential strategies for improving the stability of Sn perovskites are urgently needed.[18–21] Surface treatment of 3D perovskite with 2D perovskite is an effective way to enhance structural stability.[22,23] However, large 2D cations in the perovskite lattice hamper the charge transport, especially when the perovskite crystal structure grows parallel to the substrate.[24–26] Up to now, controlling the self-assembly processes of 2D layers into a vertical direction remains challenging. Therefore, combining superior stability and high charge transport is key to promote the development of Sn perovskite devices.

To address this issue, we demonstrate a novel approach for enhancing the stability of Sn PSCs by introducing 1,4-phenyldimethylammonium dibromide (phDMADBr), where we used phDMADBr-containing antisolvent treatment into the surface of quasi-2D Sn perovskites to form a gradient passivating layer, acting as "protective barrier" against extrinsic factors. The phDMADBr reconstructed the perovskite's surface effectively and blocked water and oxygen intrusion. This approach also leads to a highly ordered Sn perovskite film with decreased Sn(IV) content. Such surface passivation by phDMADBr effectively suppresses nonradiative recombination, promoting interfacial electron transfer. As a result, the phDMADBr-treated device achieved a maximum PCE of 11.44%. In addition, it retained over 90% of the initial efficiency for 1000 h in a N_2-filled glovebox, demonstrating the prepared devices' high efficiency and stability. Furthermore, the phDMADBr-treated device showed over 90% retention of its original efficiency exceeding 200 h in N_2 environment with a 10% RH moisture. We posit that the quasi-2D perovskite layer with a gradient passivated structure can serve as an important reference for promoting the future development of high-efficient and stable Sn PSCs.

Z. Li
School of Engineering and Materials Science (SEMS)
Queen Mary University of London
London E1 4NS, UK
M. Saliba
Helmholtz Young Investigator Group FRONTRUNNER
IEK5-Photovoltaics
Forschungszentrum Jülich
52425 Jülich, Germany

2. Results and Discussion

To reduce the rapid Sn(II) oxidation on the surface of the Sn perovskite film, we introduced phDMADBr to induce a self-assembly surface reconstruction.[15] From the molecular structure of phDMADBr (Figure S1, Supporting Information), we infer that the diammonium cation at both ends can form hydrogen bonds with the inorganic slabs, which passivate the surface, minimize gap states formation, and increase the stability of the quasi-2D perovskite structure.[27–30] Additionally, the ammonium cation and the bromide anion from phDMADBr can passivate the positive/negative charge defects and form a compact layer through N-I interaction, Sn-Br ionic bond, coordination, and hydrogen bonds. These interactions enhance the moisture and oxygen resistivity of the device.[31] Fourier transform infrared (FTIR) spectroscopy indicates stronger interaction caused by phDMADBr than Van der Waals attraction (Figure S2, Supporting Information).

To reveal the passivation effect, a first principles calculation within density functional theory (DFT) was carried out to understand the mechanism behind the passivation effect, and the corresponding models are shown in Figure S3 (Supporting Information). For the control film, FA-terminated and SnI_2-terminated optimization showed a slight geometric deformation with the I-ion downward in FAI-terminal and upward in SnI-terminal. On the phDMADBr-treated perovskite surface, a close network-like packed molecular layer is formed through Br—H, H—I interactions and Br—Sn chemical bond between phDMADBr and the perovskite surface. In particular, phDMADBr deformation occurs through phDMAD$^+$—Br$^-$—FA$^+$ interaction, effectively connecting phDMADBr to the perovskite's surface, as shown in Figure S3a (Supporting Information). For SnI_2-termination in Figure S3b (Supporting Information), Br$^-$ is bonded with uncoordinated Sn atoms, where six Br–Sn bonds are formed, leaving only two uncoordinated Sn atoms, demonstrating the outstanding capability of phDMADBr in passivation. Moreover, we observe an additional network-like structure through phDMAD$^+$—Br$^-$—Sn(II) interaction. This network-like packed molecular layer primarily serves three functions: (i) boosting electron transfers through chemical bonding rather than diffusion as well as avoiding electron accumulation; (ii) passivating undercoordinated Sn atoms and suppressing Sn(II) oxidation to Sn(IV); (iii) resisting water and oxygen erosion and enhancing perovskite's environmental stability.

To evaluate the water resistance capabilities of control perovskite and PhDMADBr-treated perovskite films, we built a model to simulate the molecular dynamics onto the perovskite film's surface (**Figure 1a,b** (SnI-terminal) and Figure S4 (Supporting Information, FAI-terminal)). For the control samples, the water layer was placed 2.6 Å above the perovskite layer. The water molecules rapidly descended by the Sn—O and I—H electrostatic interaction, then infiltrated rapidly into the perovskite layer, leading to significant geometric deformation of the perovskite surface. In contrast, on the perovskite/phDMADBr surface, most water molecules were blocked, where only 2 out of 85 molecules reached the perovskite surface through the phDMADBr molecule layer, suggesting remarkable capability in enhancing the film hydrophobicity.

**ADVANCED
SCIENCE NEWS**

www.advancedsciencenews.com

**ADVANCED
MATERIALS**

www.advmat.de
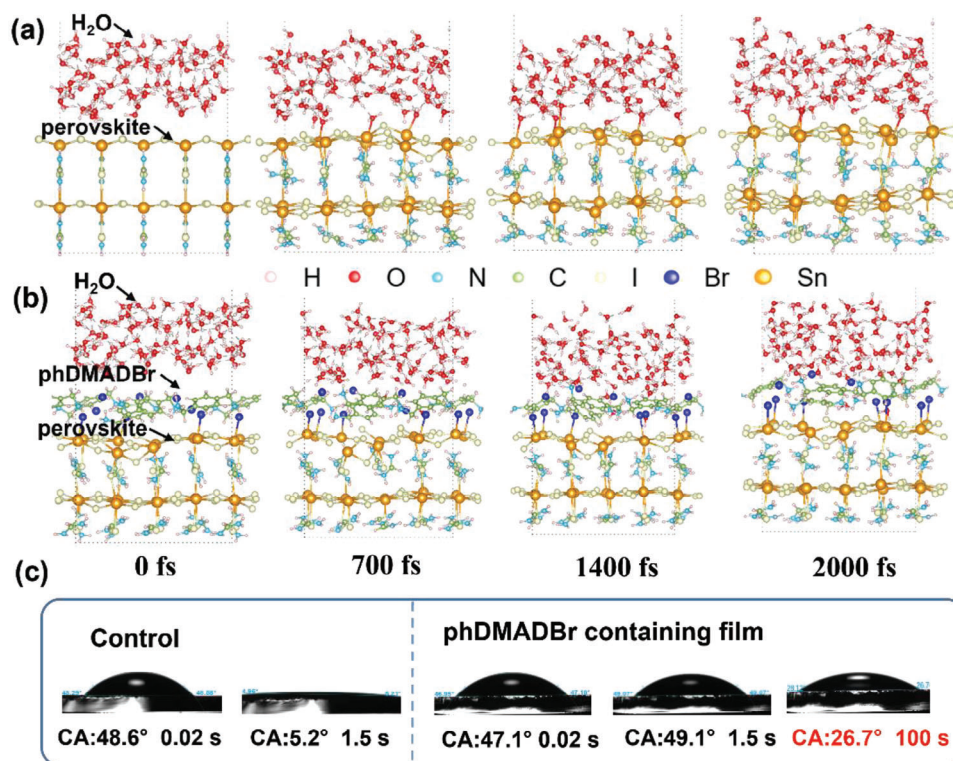
Figure 1. The evolution of the water layer on a) perovskite and b) perovskite/1,4-phenyldimethylammonium dibromide diamine (PhDMADBr) surfaces during the molecular dynamics. c) Contact angles (CAs) of water droplets on the surface of the perovskite film deposited on ITO glass directly.

To verify the hydrophobicity of the perovskite film with phDMADBr, we conducted a water contact angle (CA) tests. As shown in Figure 1c, the water drops collapsed soon after the droplet dripped, and the CA value of the control film decreased to nearly zero (the resultant value was 5.2°) within 1.5 s. On the other hand, phDMADBr significantly improved the hydrophobicity of the perovskite film, with the CA remaining over 26° even after 100 s. Figure S5 (Supporting Information) presents the CA variation for the films treated with and without phDMADBr during testing. Sharply decreased CA values indicate poor hydrophobic properties of the pristine Sn perovskite film. In addition, the surface free energy (SFE) obtained from the hydrophobicity tests was also used to evaluate the thermodynamic stability of perovskites.[32,33] From Figure S5 (Supporting Information), we observe that perovskite film treated with phDMADBr possessed lower SFE (60.49 mN m^{-1}) than that of the control film (70.84 mN m^{-1}), indicating superior thermodynamical stability of the treated films.[34]

In situ X-ray photoelectron spectroscopy (XPS) was employed to investigate the suppression of Sn(II) oxidation by phDMADBr-induced surface reconstruction in a humid environment. The perovskite films were exposed to 50% RH atmosphere before each XPS measurement to track the changes in Sn's valence state. As shown in **Figure 2a,b**, the Sn 3d7/2 core XPS spectrum of the pristine FASnI$_3$ perovskite film showed two divided peaks at 487.2 and 488.1 eV, associated with the signals of Sn(II) in perovskite lattice and oxidized Sn(IV) species on the film surface, respectively.[35] Initially (0 min), there were no significant differences in the Sn(II) content (87.3% for the control sample

and 89.1% for the target sample, respectively). After 10 min, the Sn(II) content in the control sample decrease significantly. After 1 h, the Sn(II) content of the control film had fallen to only 31.9%. In contrast, in the phDMADBr-treated perovskite films, the content of Sn(II) remained at 63.7%. Detailed data of Sn(II) contents are shown in Figure 2c and Table S1 (Supporting Information). Notably, that the initial Sn(II) percentage of the film is less than 100% due to the ex situ XPS testing, involving multiple steps from sample preparation to testing, potentially leading to the Sn(II)'s oxidization. In addition, the zero point of the x-axis in Figure 2c represents the initiation of the test timeframe. phDMADBr decreased the Sn(II) oxidation rate significantly, which suggests that the surface reconstruction caused by phDMADBr enhances the film's water stability.

In addition, we employed field emission scanning electron microscope (FE-SEM) to analyze the moisture stability of perovskite crystal morphologies. Figure 2d,e shows the initial morphology of perovskite films with and without phDMADBr, respectively. After exposing the samples to air with 35% RH for 1 h, the pristine film exhibited severe surface degradation, including structural collapse and many voids across perovskite film, especially at the grain boundaries (Figure 2f). In contrast, no visible crystal voids or pinholes at grain boundaries were observed for the phDMADBr-treated perovskite films (Figure 2g). The degradation conducted under the higher relative humidity (80% RH) demonstrated that phDMADBr could effectively prevent water molecules from penetrating the perovskite film (Figure S6, Supporting Information).
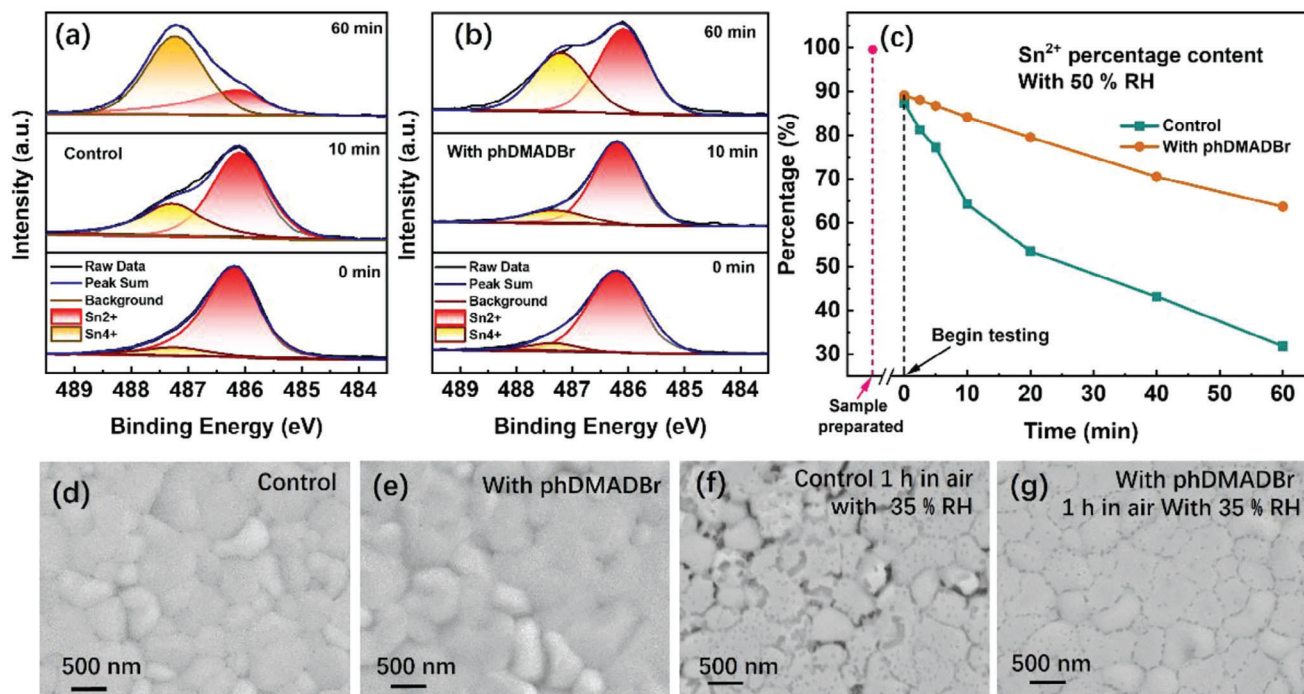
Figure 2. Stability of perovskite films against moisture. a) In situ Sn element X-ray photoelectron spectroscopy (XPS) spectra of the control sample. b) XPS spectra of samples treated with 1,4-phenyldimethylammonium dibromide diamine (phDMADBr), the Sn(II) content is more than the control device. c) Sn(II) percentage evolution with time in the perovskite film with and without phDMADBr, where perovskite films degenerated in the 50% RH atmosphere after each XPS testing. d,e) Field emission scanning electron microscope (FE-SEM) images of Sn perovskite films with and without phDMADBr without air contact. f,g) The control and the target films were exposed to air with 35% RH for 60 min.

We performed grazing incidence wide-angle X-ray scattering (GIWAXS) based on synchrotron radiation to probe and understand the surface remodeling process upon treatment with phDMADBr. **Figure 3** displays the 2D GIWAXS patterns of the control and phDMADBr-treated samples at different stages, from spin-coating to annealing completion. The perovskite crystallization process starts only upon dripping the antisolvent, as indicated by the appearance of the diffraction peak at $10 \, \text{nm}^{-1}$ in the GIWAXS pattern (Figure S7, Supporting Information). By comparing the GIWAXS pattern shown in Figure S8a,e (Supporting Information), we observed an intense peak in the control film, revealing a faster initial crystallization rate than the target sample. As the annealing time continued, the diffraction peak increased. After annealing for 100 s, the peaks representing the quasi-2D perovskite emerged at about $q = 3$ and $4 \, \text{nm}^{-1}$. However, the peaks belonging to the quasi-2D perovskite of the control film faded with increasing annealing time (Figure S8c,d, Supporting Information). Also, these two diffraction peaks of the phDMADBr-treated perovskite films remained until the annealing process completion. Video S1 (Supporting Information) visually displays the crystallization process of perovskite films. These results demonstrate the effectiveness of phDMADBr in protecting the quasi-2D structure on the surface of the perovskite, thereby increasing the stability of the film.

To systematically investigate the mechanism of the surface reconstruction in phDMADBr-treated perovskite films, we plotted false-color intensity maps as a function of wave vector q and time (with 2 s frame rate) during both spin-coating and annealing pro-

cesses, as presented in Figure 3a,b. The spin-coating time ranged from 0 to 70 s, and the annealing time ranged from 70 to 300 s. The scattering halos that appeared at ≈60 s is blurred, owing to the rapid volatilization of residual solvents, with the phase transition of the perovskite crystal.[36] The scattering halos of the perovskite are mainly distributed around $q = 10$ and $20 \, \text{nm}^{-1}$. Notably, the beginning of the integrated curve ($q = 10 \, \text{nm}^{-1}$) presented sharp characteristics, indicating the altered crystallization mode by introducing phDMADBr. Additionally, the signal at $q = 2.8 \, \text{nm}^{-1}$ represents a quasi-2D phase, which starts appearing at about 60 s and continues till the end of the process. We suggest that the compact film protects the quasi-2D phase on the surface of the perovskite film through Br–Sn chemical bond. Comparing the two samples, we found that the target film showed a longer uniform diffraction intensity forming time than the control one, revealing that phDMADBr slowed the crystallization rate. The data in Figure 3c recorded the phDMADBr's functions on the surface reconstruction dynamics. The annealing was started at $t = 70$ s, the initial annealing process was accompanied by further crystallization of perovskite. It distinctly presents in the curves that the peak areas (100) of the control sample keep increasing until 80 s, indicating that the perovskite film's crystallization is complete. In contrast, the crystallization process of the phDMADBr-treated sample lasted until 122 s. A lower crystallization rate benefits crystal growth, achieving a compact film, and reducing the defect ratio. It also enables more uniformly complete nucleation sites, leading to a flat, less-defective film.[37]
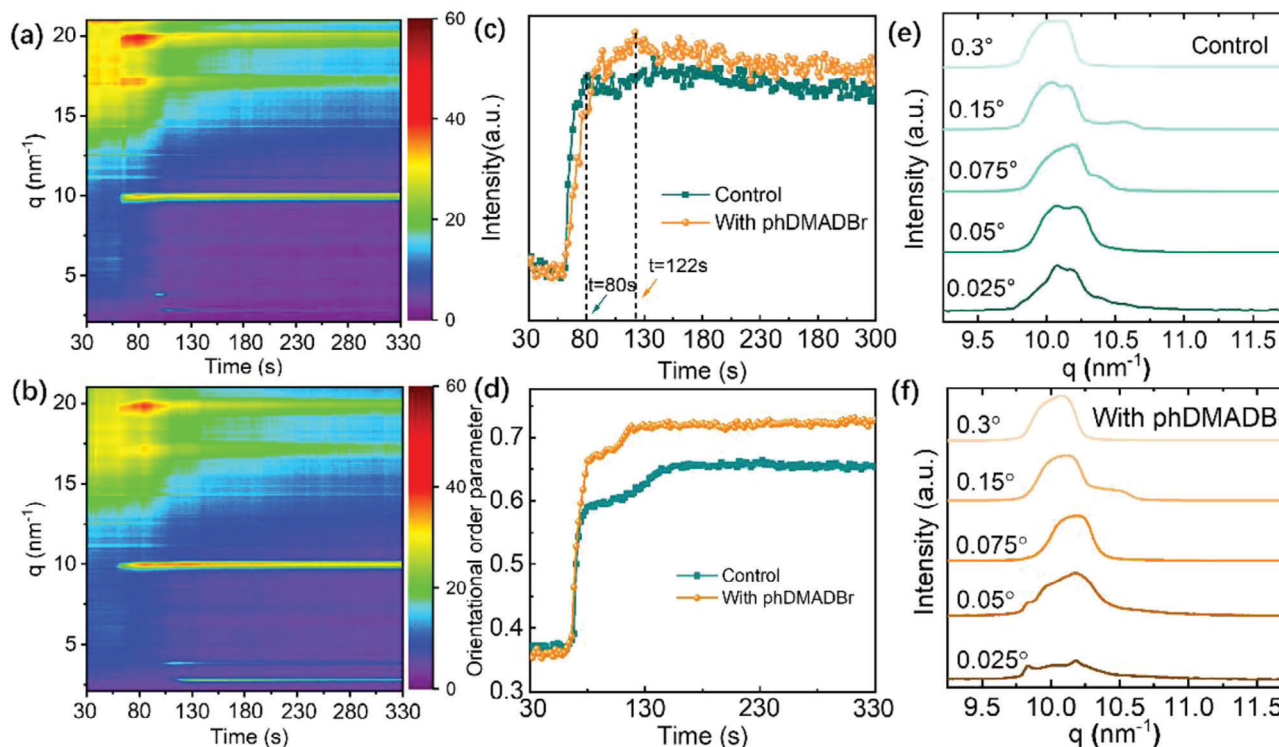
Figure 3. Crystallization kinetics of perovskite film via in situ grazing incidence wide-angle X-ray scattering (GIWAXS) analysis. a) Time-resolved azimuthally integrated intensity patterns for control and b) 1,4-phenyldimethylammonium dibromide diamine (phDMADBr) treated perovskite films. c) Time-dependent diffraction of peak area of perovskite (100) crystal plane. The dashed lines show the curve's turning point, representing the crystallization ending time. d) Orientational order of the perovskite crystal as a function of time. e) The (100) crystal surface peak area of GIWAXS with different incident angles for control and f) phDMADBr-treated perovskite films.

In Figure 3d, we recorded the variations in the orientational order of the perovskite crystal during the spin-coating and annealing processes. The curve of the phDMADBr-treated film shows an increasingly higher crystal orientation than the control samples. Furthermore, the orientation order parameter S of the control perovskite film stabilized at around 0.64, while the S value of the treated film with phDMADBr is over 0.72, suggesting an increased preferred orientation. The increase in S value verifies that phDMADBr treatment promotes an improved orientation of the Sn perovskite crystals. Next, we further track the crystallization process for analyzing the radially integrated azimuth intensity patterns along the ring at $q = 10$ nm^{-1} (Figure S9, Supporting Information). Our results indicate a preferential crystal orientation at the azimuth of 90° in the perovskite films, which promotes charge transport along the out-of-plane direction. The enhanced intensity proves that the phDMADBr treatment significantly promotes the crystallographic orientation.[38,39] The Sn-based perovskites' preferred crystal orientation can improve their charge transport.[40]

The crystal structure evolution during annealing was monitored and shown in Figure S10 (Supporting Information), which shows q-dependent 1D-GIXRD spectra obtained from 2D-GIWAXS images. With increasing annealing time, the diffraction peaks shifted towards higher q values due to the volatilization of DMSO solvent, resulting in a contraction of the lattice spacing d.

To investigate the vertical distribution of phDMADBr within the treated perovskite films, we conducted GIWAXS measurements at variable incidence angles ranging from 0° to 0.3° (Figure S11, Supporting Information). We calculated the (100) crystal surface peak area of control and phDMADBr-treated perovskite films (Figure 3e,f). At low incidence angles, such as 0.025°, the X-ray penetration depth only detect the surface structure of the perovskite film.[41] We found that the phDMADBr-treated sample possessed a significantly weaker peak area and intensity than the control sample, indicating that phDMADBr-mediated different upper surface structures. With the increase of the incident angle, the peak area of both samples increased, among which the phDMADBr-treated sample exhibited a sharper peak shape. Notably, at an incident angle of 0.075°, the peak area of the phDMADBr-treated film exceeded that of the control sample, as exhibited in Figure S12 (Supporting Information). As the peak intensity variation correlates with the functionalization of phDMADBr for perovskite film, these intensity distribution results reveal a gradient distribution of phDMADBr along the perovskite film's shallow surface, contributing to the surface reconstruction.

To verify the effect of phDMADBr-treated Sn perovskite films, herein, we fabricated solar cells based on an inverted p-i-n architecture (Figure S1, Supporting Information). **Figure 4a,b** displays the champion devices' current density-voltage (J–V) curves obtained from the forward and reverse scans with and without phDMADBr (1 mmol mL^{-1}). The phDMADBr-treated device has
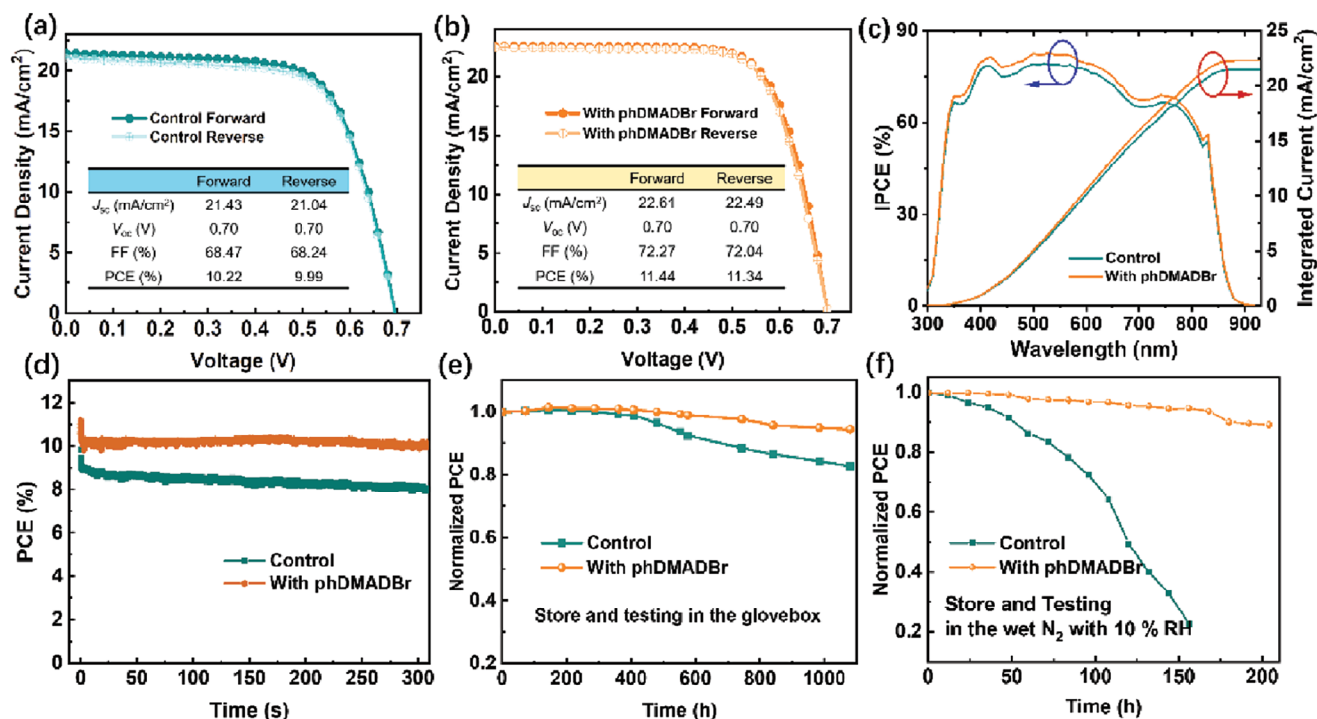
Figure 4. J–V characteristic of the control a) and target b) devices. c) Incident photon-to-current conversion efficiency (IPCE) and the integrated current of the FASnI$_3$ perovskite solar cels (PSCs) with and without 1,4-phenyldimethylammonium dibromide diamine (phDMADBr) treatment. d) Stability dependence of times at a preset maximum power point (MPP) voltage. e) Long-term stability of unencapsulated control and phDMADBr-treated PSCs stored and tested in a N$_2$-filled glovebox. f) Long-term stability of unencapsulated PSCs stored and tested in N$_2$ humid environment (25 °C, 5% < RH < 10%).

a maximum PCE of 11.44% with an open circuit voltage (V_{oc}) of 0.70 V, a short circuit current density (J_{sc}) of 22.61 mA cm^{-2} and a fill factor (FF) of 72.27% under AM 1.5G (100 mW cm^{-2}) illumination, which are higher than those of the control device (PCE of 10.22%, V_{oc} of 0.70 V, J_{sc} of 21.43 mA cm^{-2} and FF of 68.47%). The photovoltaic performance with forward and reverse sweeps of the control and phDMADBr-treated perovskite device are summarized in Table S2 (Supporting Information).

Figure 4c shows the incident photon-to-current conversion efficiency (IPCE) spectra and the corresponding integrated current. Remarkably, the device with phDMADBr exhibited higher IPCE values. The integrated current densities from IPCE were calculated to be 22.31 and 20.78 mA cm^{-2} for target and control devices, respectively. The increased current density is attributed to the suppressed nonradiative recombination and the enhancement of the carrier extraction by introducing phDMADBr on the surface of the perovskite. The increasing absorption spectra indicates that introducing phDMADBr is beneficial for enhancing the photocurrent (Figure S13, Supporting Information). These results are consistent with the J_{SC} obtained from the J–V curves. In addition, a slight increasing PL intensity (Figure S14, Supporting Information), the greater recombination resistance in the Nyquist plot (Figure S15, Supporting Information), the lower dark current density (Figure S16, Supporting Information), and the higher quasi-Fermi level splitting (QFLS) histogram (Figure S17, Supporting Information) are all confirmed that phDMADBr introduced on the surface of the perovskite can effectively suppress the surface nonradiative recombination.[42–44] Furthermore, the photovoltaic performance was reproduced by for-

ward scanning testing 20 individual control and phDMADBr-treated PSCs (Figure S18, Supporting Information). As indicated by the statistical results, phDMADBr-treated devices show better reproducibility.

The champion device treated with phDMADBr has a steady-state PCE of 11.44% over a period of 600 s at the maximum power point (MPP) voltage of 0.54 V (Figure 4d), corresponding to the light-soaking stability. Devices durability as a function of storage period is shown in Figure 4e. Stability testing was carried out for over 1000 h in a N$_2$-filled glovebox. The phDMADBr-treated device retained over 90% of its initial PCE beyond 1000 h. However, the PCE of the control device declined dramatically after 400 h. Additional tests were conducted on control and target devices for several weeks by storing them in the moisture buster cabinet (10% RH, inert atmosphere) (Figure 4f). Despite a slight decrease, the target device maintained 90% of its initial PCE for over 200 h. However, the control device degraded clearly within 24 h, whose PCE decreased below 20% at about 150 h. These indicated that the functionalization of phDMADBr improves the humidity stability of Sn PSCs.

3. Conclusion

In this work, we introduced phDMADBr-based diamine compounds into the Sn perovskite absorber layer using an antisolvent crystallization method, and the well-defined surface reconstruction of the perovskite films was realized successfully. The network-like packed molecules film firmly combined with the perovskite surface through chemical bonding interactions of

Br—Sn and Br—H. Such a unique structure provides resistance against water aggression and holds the quasi-2D perovskite layer in position well. The resultant perovskite film exhibited enhanced crystal structure stability, reduced defect states, and facilitated interfacial charge transfer. With the films, we remarkably enhanced stability in Sn PSCs with a PCE of 11.44%, retaining 90% of the initial efficiency after storage under N_2 atmosphere for over 1000 h and retaining 90% of the original efficiency in a 10% RH environment for more than 200 h. This work highlights surface reconstruction as an effective approach for enhancing perovskite structure stability that can engineer the device's operational durability. It will set the foundation for advancing lead-free Sn PSCs into the photovoltaic market.

Supporting Information

Supporting Information is available from the Wiley Online Library or from the author.

Conflict of Interest

The authors declare no conflict of interest.

Data Availability Statement

Research data are not shared.

[1] J. J. Yoo, G. Seo, M. R. Chua, T. G. Park, Y. Lu, F. Rotermund, Y.-K. Kim, C. S. Moon, N. J. Jeon, J.-P. Correa-Baena, V. Bulovic, S. S. Shin, M. G. Bawendi, J. Seo, *Nature* **2021**, *590*, 587.

[2] M. Kim, J. Jeong, H. Lu, T. K. Lee, F. T. Eickemeyer, Y. Liu, I. W. Choi, S. J. Choi, Y. Jo, H.-B. Kim, S.-I. Mo, Y.-K. Kim, H. Lee, N. G. An, S. Cho, W. R. Tress, S. M. Zakeeruddin, A. Hagfeldt, J. Y. Kim, M. Grätzel, D. S. Kim, *Science* **2022**, *375*, 302.

[3] R. He, W. Wang, Z. Yi, F. Lang, C. Chen, J. Luo, J. Zhu, J. Thiesbrummel, S. Shah, K. Wei, Y. Luo, C. Wang, H. Lai, H. Huang, J. Zhou, B. Zou, X. Yin, S. Ren, X. Hao, L. Wu, J. Zhang, J. Zhang, M. Stolterfoht, F. Fu, W. Tang, D. Zhao, *Nature* **2023**, *618*, 80.

[4] M. Lyu, J.-H. Yun, P. Chen, M. Hao, L. Wang, *Adv. Energy Mater.* **2017**, *7*, 1602512.

[5] M. Ren, X. Qian, Y. Chen, T. Wang, Y. Zhao, *J. Hazard. Mater.* **2022**, *426*, 127848.

[6] Y. Takahashi, R. Obara, Z.-Z. Lin, Y. Takahashi, T. Naito, T. Inabe, S. Ishibashi, K. Terakura, *Dalton Trans.* **2011**, *40*, 5563.

[7] F. Zuo, S. T. Williams, P.-W. Liang, C.-C. Chueh, C.-Y. Liao, A. K.-Y. Jen, *Adv. Mater.* **2014**, *26*, 6454.

[8] X. Jiang, H. Li, Q. Zhou, Q. Wei, M. Wei, L. Jiang, Z. Wang, Z. Peng, F. Wang, Z. Zang, K. Xu, Y. Hou, S. Teale, W. Zhou, R. Si, X. Gao, E. H. Sargent, Z. Ning, *J. Am. Chem. Soc.* **2021**, *143*, 10970.

[9] H. Shi, D. Han, S. Chen, M.-H. Du, *Phys. Rev. Mater.* **2019**, *3*, 034604.

[10] X. Zhang, S. Wang, W. Zhu, Z. Cao, A. Wang, F. Hao, *Adv. Funct. Mater.* **2021**, *32*, 2108832.

[11] J. Pascual, G. Nasti, M. H. Aldamasy, J. A. Smith, M. Flatken, N. Phung, D. Di Girolamo, S.-H. Turren-Cruz, M. Li, A. Dallmann, R. Avolio, A. Abate, *Mater. Adv.* **2020**, *1*, 1066.

[12] A. Abate, *ACS Energy Lett.* **2023**, *8*, 1896.

[13] Y. Yin, M. Wang, V. Malgras, Y. Yamauchi, *ACS Appl. Energy Mater.* **2020**, *3*, 10447.

[14] K. Nishimura, M. A. Kamarudin, D. Hirotani, K. Hamada, Q. Shen, S. Iikubo, T. Minemoto, K. Yoshino, S. Hayase, *Nano Energy* **2020**, *74*, 104858.

[15] H. Li, B. Chang, L. Wang, Z. Wang, L. Pan, Y. Wu, Z. Liu, L. Yin, *ACS Energy Lett.* **2022**, *7*, 3889.

[16] X. Li, M. I. Dar, C. Yi, J. Luo, M. Tschumi, S. M. Zakeeruddin, M. K. Nazeeruddin, H. Han, M. Grätzel, *Nat. Chem.* **2015**, *7*, 703.

[17] E. Jokar, C.-H. Chien, C.-M. Tsai, A. Fathi, E. W.-G. Diau, *Adv. Mater.* **2019**, *31*, 1804835.

[18] S. Ma, G. Yuan, Y. Zhang, N. Yang, Y. Li, Q. Chen, *Energy Environ. Sci.* **2022**, *15*, 13.

[19] J. Zhou, M. Hao, Y. Zhang, X. Ma, J. Dong, F. Lu, J. Wang, N. Wang, Y. Zhou, *Matter* **2022**, *5*, 683.

[20] S. Li, Z. He, Y. Li, K. Liu, M. Chen, Y. Yang, X. Li, *J. Alloys Compd.* **2021**, *889*, 161561.

[21] Y.-W. Jang, S. Lee, K. M. Yeom, K. Jeong, K. Choi, M. Choi, J. H. Noh, *Nat. Energy* **2021**, *6*, 63.

[22] M. Seitz, P. Gant, A. Castellanos-Gomez, F. Prins, *Nanomaterials* **2019**, *9*, 1120.

[23] X. Yue, X. Zhao, B. Fan, Y. Yang, L. Yan, S. Qu, H. Huang, Q. Zhang, H. Yan, P. Cui, J. Ji, J. Ma, M. Li, *Adv. Funct. Mater.* **2022**, *33*, 2209921.

[24] A. Chen, M. Shiu, J. H. Ma, M. R. Alpert, D. Zhang, B. J. Foley, D.-M. Smilgies, S.-H. Lee, J. J. Choi, *Nat. Commun* **2018**, *9*, 1336.

[25] M. Li, W.-W. Zuo, Y.-G. Yang, M. H. Aldamasy, Q. Wang, S. H. T. Cruz, S.-L. Feng, M. Saliba, Z.-K. Wang, A. Abate, *ACS Energy Lett.* **2020**, *5*, 1923.

[26] J. Zhao, Z. Zhang, G. Li, M. H. Aldamasy, M. Li, A. Abate, *Adv. Energy Mater.* **2023**, *13*, 2204233.

[27] X. Meng, Y. Li, Y. Qu, H. Chen, N. Jiang, M. Li, D.-J. Xue, J.-S. Hu, H. Huang, S. Yang, *Angew. Chem.* **2021**, *133*, 3737.

[28] S. Ahmad, P. Fu, S. Yu, Q. Yang, X. Liu, X. Wang, X. Wang, X. Guo, C. Li, *Joule* **2019**, *3*, 794.

[29] L. Mao, W. Ke, L. Pedesseau, Y. Wu, C. Katan, J. Even, M. R. Wasielewski, C. C. Stoumpos, M. G. Kanatzidis, *J. Am. Chem. Soc.* **2018**, *140*, 3775.

[30] P. Huang, S. Kazim, M. Wang, S. Ahmad, *ACS Energy Lett.* **2019**, *4*, 2960.

[31] X. Li, W. Ke, B. Traoré, P. Guo, I. Hadar, M. Kepenekian, J. Even, C. Katan, C. C. Stoumpos, R. D. Schaller, M. G. Kanatzidis, *J. Am. Chem. Soc.* **2019**, *141*, 12880.

[32] J. M. Mchale, A. Auroux, A. J. Perrotta, A. Navrotsky, *Science* **1997**, *277*, 788.

[33] H. Zhou, F. Wang, Y. Wang, C. Li, C. Shi, Y. Liu, Z. Ling, *RSC Adv.* **2021**, *11*, 5512.

[34] S. Wang, X. Huang, L. Liu, P. Yan, Y. Chen, F. Fang, J. Guo, *J. Environ. Manage.* **2021**, *298*, 113521.

[35] L. Rao, X. Meng, S. Xiao, Z. Xing, Q. Fu, H. Wang, C. Gong, T. Hu, X. Hu, R. Guo, Y. Chen, *Angew. Chem., Int. Ed.* **2021**, *133*, 14814.

[36] M. Wang, W. Tian, F. Cao, M. Wang, L. Li, *Adv. Funct. Mater.* **2020**, *30*, 1909771.

[37] D. Huang, P. Xie, Z. Pan, H. Rao, X. Zhong, *J. Mater. Chem. A* **2019**, *7*, 22420.

[38] G. Li, Z. Su, M. Li, F. Yang, M. H. Aldamasy, J. Pascual, F. Yang, H. Liu, W. Zuo, D. Di Girolamo, Z. Iqbal, G. Nasti, A. Dallmann, X. Gao, Z. Wang, M. Saliba, A. Abate, *Adv. Energy Mater.* **2021**, *11*, 2101539.

[39] J. Song, G. Zhou, W. Chen, Q. Zhang, J. Ali, Q. Hu, J. Wang, C. Wang, W. Feng, A. B. Djurisic, H. Zhu, Y. Zhang, T. Russell, F. Liu, *Adv. Mater.* **2020**, *32*, 2002784.

[40] L. Ji, D. Liu, Y. Wang, T. Zhang, H. Chen, Y. Li, H. Zheng, Y. Yang, Z. David Chen, W. Yang, L. Chen, S. Li, *Chem. Eng. J.* **2020**, *402*, 125133.

[41] S. Sidhik, Y. Wang, M. De Siena, R. Asadpour, A. J. Torma, T. Terlier, K. Ho, W. Li, A. B. Puthirath, X. Shuai, A. Agrawal, B. Traore, M. Jones, R. Giridharagopal, P. M. Ajayan, J. Strzalka, D. S. Ginger, C. Katan, M. A. Alam, J. Even, M. G. Kanatzidis, A. D. Mohite, *Science* **2022**, *377*, 1425.

[42] F. Qi, X. Deng, X. Wu, L. Huo, Y. Xiao, X. Lu, Z. Zhu, A. K.-Y. Jen, *Adv. Energy Mater.* **2019**, *9*, 1902600.

[43] Z. Li, J. Zhang, S. Wu, X. Deng, F. Li, D. Liu, C.-C. Lee, F. Lin, D. Lei, C.-C. Chueh, Z. Zhu, A. K.-Y. Jen, *Nano Energy* **2020**, *78*, 105377.

[44] J. K. Katahara, H. W. Hillhouse, *J. Appl. Phys.* **2014**, *116*, 173504.